Lateral confinement of laser ablation plasma in magnetic field

C Pagano, J G Lunney

Lateral confinement of laser ablation plasma in magnetic field

C Pagano and J G Lunney
School of Physics, Trinity College Dublin, Dublin 2, Ireland.

Abstract. The expansion of copper laser produced plasma along a magnetic field was investigated with the aim of confining the lateral expansion of the plasma. Time-resolved optical imaging, time- and space-resolved optical emission spectroscopy and time-of-flight Langmuir ion probe measurements were used to study the plasma dynamics. Thin films of copper were deposited without, and with, the magnetic field. It was observed that the magnetic field gives rise to substantial confinement of the plasma, leading to an increase by a factor of 6 in the ion yield and 2.6 in the deposition rate.

1. Introduction

The laser ablation process is widely used in applications such as laser micromachining, laser induced breakdown spectroscopy (LIBS) for material analysis and pulsed laser deposition (PLD) of thin films. For some of these applications it would be beneficial to reduce the lateral expansion of the ablation plume, leading to a more forward-directed expansion. When the ablation material is significantly ionised, it is expected that the moving plasma will interact with a static magnetic field. There are several reports of experiments where a magnetic field has been demonstrated to strongly influence the flow of laser produced plasma.

In PLD a curved solenoidal magnetic field of moderate strength (~100 mT) has been used to guide the plasma on a curved path between target and substrate and thus avoid particulate contamination [1]. Permanent magnets have also been used to deflect the laser produced plasma (LPP) [2 - 5]. Kobayashi et al. [6] demonstrated that placing a permanent magnet behind the substrate leads to an increase of the spectral emission from ions in the LPP and improves the PLD of high temperature superconductor. Rai et al. [7] studied the emission properties of LPP from both solid and liquid targets expanding across a magnetic field with the aim of enhancing the sensitivity of the LIBS system. Both Harilal et al. [8] and L. Dirnberger et al. [9] also studied the expansion of LPP across a magnetic field and observed enhanced emission from ionized species. This was qualitatively explained in terms of a magnetohydrodynamic (MHD) model of the interaction of the moving plasma with the field. According to this model, the increase in the state of excitation of the plume is due to Joule heating by the induced current density $\boldsymbol{J}$. Pagano et al. [10] also studied the influence of a transverse magnetic field on LPP and found that the forward expansion is reduced and the spectral emission is modified by the magnetic field. Pisarczyk et al. [11] studied the flow of much hotter LPP along a strong magnetic field (~20 T), with the aim of laterally confining the plasma for soft X-ray laser development. A miniature magnetic cusp configuration has also been suggested for confinement of plasma produced by femtosecond laser with a view to increasing the neutron yield [12].

This paper describes the results of experiments to investigate the flow of a low temperature copper LPP in a magnetic field where the target normal lies parallel to the magnetic field lines. Time resolved imaging of the plasma self-emission clearly showed that the magnetic field limits the lateral expansion in comparison with the free ablation case. Consequently, in presence of the magnetic field, a much higher deposition rate was measured, which is of interest in PLD.

2. Experimental methods

The magnetic field for this experiment was produced by 2 Nd-Fe-B ring magnets attached to an iron yoke as shown in figure 1. The dimensions of each magnet were: 20 mm height, 45 mm external diameter and 15 mm diameter hole. The distance between the magnets was 35 mm. The origin of the coordinate system used to describe the field is taken to be on the axis of the system and midway between the magnets, as shown in figure 1. The magnet configuration was designed using the

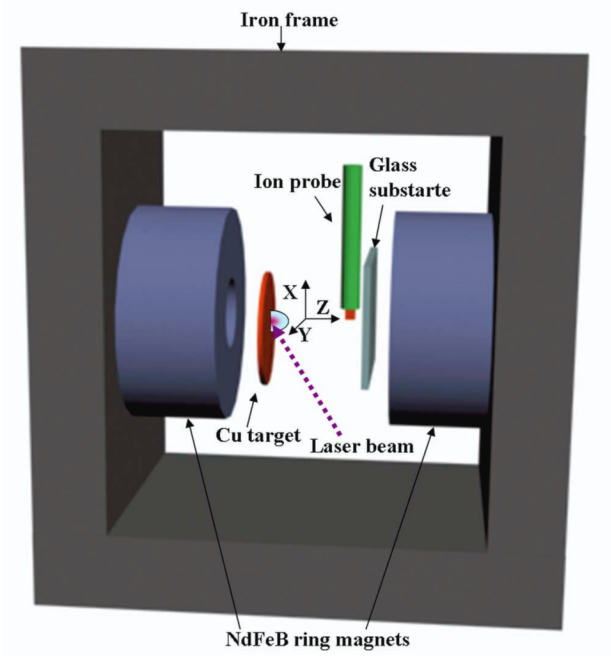

Figure 1: Schematic of the experimental set-up.

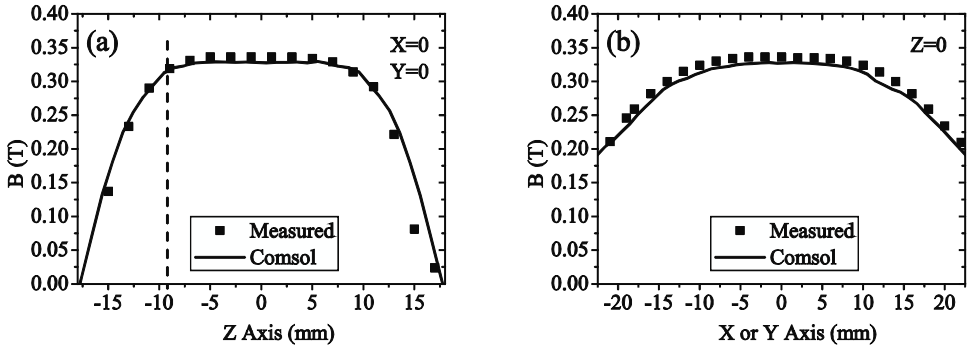

Figure 2: Comparison between the measured and calculated magnetic profile. The origin of the coordinate system lies on the axis midway between the magnets.

COMSOL MULTIPHYSICS computer code [13]. Figure 2(a) shows the variation of the field along the *Z* direction for $X = Y = 0$ and figure 2(b) shows the variation in the *X* or *Y* direction at $Z = 0$. The calculated field profiles agree closely with Hall probe measurements. Along the *Z* direction the field increases rapidly from a value of 11 mT at the magnet surface to 320 mT at 8 mm from the surface and remains constant at this value over a region spanning 20 mm. The copper (Cu) target was placed at 8 mm from the surface of one of the magnets ($Z = -9.5$ mm) as indicated by the vertical line in figure 2(a). Thus the plasma is produced in, and expands into, a region of uniform field.

A 248 nm, 20 ns excimer laser was used to irradiate a Cu target in a stainless steel vacuum chamber, at pressure of about 10^{-4} mbar. The laser spot area was 0.02 cm^2 giving a fluence of ~4 J/cm^2. The target was rotated to reduce drilling. The influence of the magnetic field on the plasma flow was investigated as follows. The ion flux was measured using a negatively biased (-10 V), 2×2 mm^2 planar ion probe placed on the *Z* axis at 2 cm from the target and oriented to face the target. Time resolved optical imaging and time- and space-resolved optical emission spectrometry of the plasma self-emission was also used viewing the plasma in the *Y*-direction, i.e. orthogonal to the target normal. The time resolved optical imaging shows the evolution of the shape of the plasma plume and it was done with an intensified charge coupled device (ICCD) with a minimum gate time of 2 ns. For the emission spectrometry, a single converging lens was used to form a ×0.154 demagnified image of

the plume on the slit of an Oriel MS260i imaging spectrometer. A periscope was used to orient the plume image so that the direction corresponding to the target normal lies along the slit. The imaging system in the spectrometer has a magnification of ×1.6. The spectrometer was equipped with a 300 lines/mm grating which gives spectral resolution of 0.75 nm and ICCD detector with a minimum gate time of 5 ns. The spectral range was 360 – 600 nm. The absolute spectral sensitivity of the overall spectrometric system was calibrated using an Oriel 6333 100 W quartz halogen lamp. Both the ICCDs used in this experiment were triggered to record the emission simultaneously and at various time delays after the laser has fired. At each time delay the background was acquired and subtracted from the corresponding emission signal. Furthermore depositions on glass substrates were made at 2 cm from the target to investigate how the magnetic field influences the amount and spatial distribution of ablated material. It should be noted that the glass substrate was not present during the acquisition of the plasma images.

3. Results and discussion

At first, the mass ablated per pulse was measured in both cases, without and with the magnetic field. Keeping the target stationary, a small crater was formed in the Cu target with 1000 laser shots. The crater was scanned using a surface profiler and the ablation mass per pulse estimated. The ablation spot was nearly elliptical with minor and major diameters of 1.25 mm and 2.1 mm, respectively. The maximum ablation depth per pulse was ~16 nm. Without the magnetic field the number of atoms ablated per shot was $(1.6\pm0.1)\text{x}10^{15}$ and with the magnetic field was $(1.8\pm0.1)\text{x}10^{15}$; thus, within the accuracy of the measurement, the field does not influence the amount of material ablated.

Figure 3(a) shows the ion current per unit area at 2 cm from the target recorded on the Langmuir ion probe for both free ablation and in the presence of a magnetic field. In a vacuum environment, without magnetic field, the ion flux measured can be understood in terms of the adiabatic, isentropic expansion model developed by Anisimov et al. [14, 15]. At the end of the laser pulse the ablated material exists as a thin layer of plasma on the target surface. The steep density gradients give rise to rapid acceleration. After a short distance, of about 3 times the ablation spot diameter, the plume acceleration is complete and the semi-ellipsoidal plume expands inertially while remaining self-similar. The plume elongation in the forward direction is described by the aspect ratios $k_x = Z/X$ and $k_y = Z/Y$, where Z is the position of the plume front normal to the target surface and X and Y are the positions in the directions parallel to the target surface.

When the target-probe distance (D) is much larger than the ablation spot diameter the plasma flow at the probe position is inertial, and the ion flow velocity is to a good approximation given by D divided by the ion time-of-flight (TOF) measured from the time of laser irradiation. In figure 3(a) the TOF at the maximum ion flux for the free ablation is 1.2 μs, which corresponds to an ion velocity of 1.7×10^6 cm s^{-1} and ion energy of 94 eV. Since the ion current density measured by the probe is given by the product of ion density and flow velocity, it may be used to find the temporal variation of ion density at the probe position [15, 16]. Furthermore, since the expansion is self-similar, ion probe signal can also be used to estimate the plasma density profile at any distance from the target as a function of time, otherwise, for a given time, to extract the density as a function of the distance [10]. As an example, figure 3(b) shows the density at 600 ns derived from the ion signal for free ablation. Indeed the ion TOF signal may be used to find the ion energy distribution through the following equation:

$$\frac{\mathrm{d}N}{\mathrm{d}E} = -\frac{It^3}{eAmD^2} \qquad (1)$$

where dN/dE is the number of ions per unit area and energy interval, in eV, I/A is the ion current density collected by the probe (A being the probe area), t is the time, m is the ion mass and e is the electron charge. The ion energy distribution on axis is shown in figure 3(c); it can be seen that the ion energies range up to ~200 eV and the average energy is about 63 eV.

Figure 3(a) also shows the ion probe signal at 2 cm in the presence of the axial magnetic field. The peak ion current density is 6 times higher than the free ablation case, indicating substantial concentration of the plasma flow in the forward direction. Since the magnetic field is normal to the surface of the probe, it should not significantly influence the ion signal due to plasma flow along the

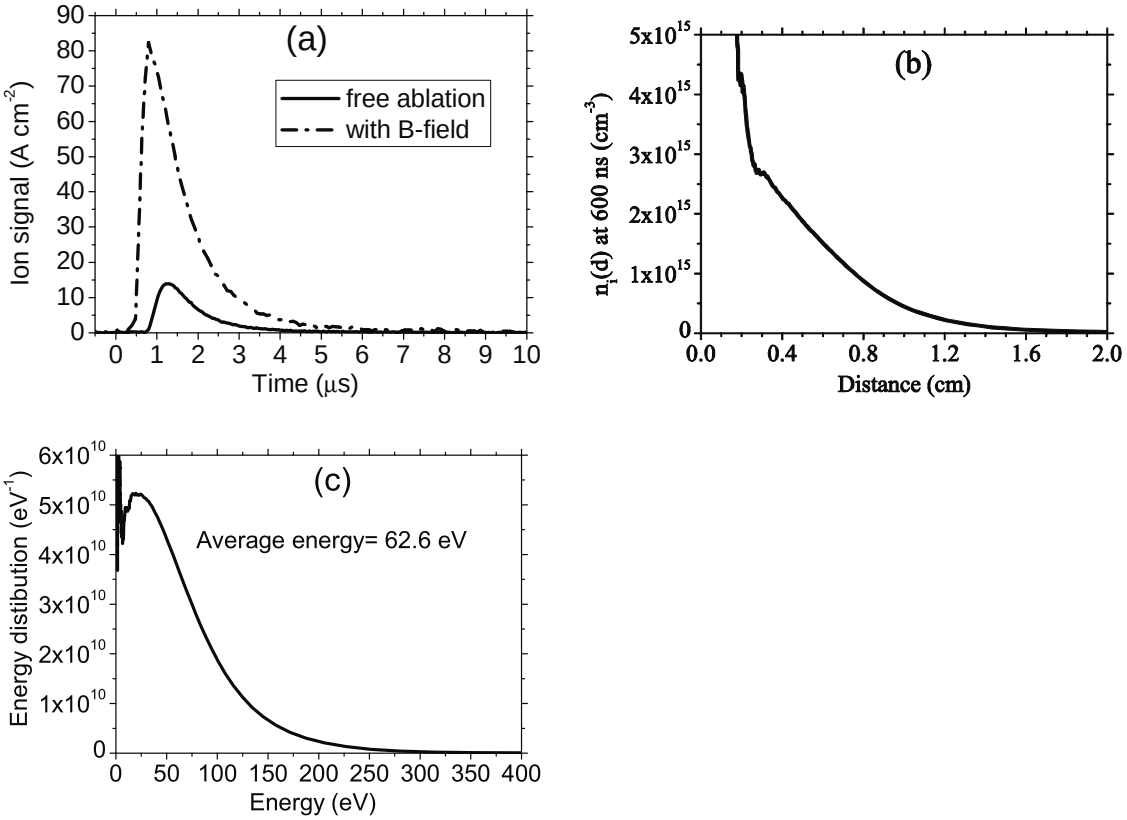

Figure 3: (a) Ion time of flight signal acquired with Langmuir probe at 2 cm from the target, at a laser fluence of 3 J/cm^2; **(b)** corresponding ion density profile at 600 ns as function of the distance from the target; **(c)** ion energy distribution.

field lines. Assuming the ions are mainly singly charged, the signals in figure 3(a) can be used to find the number of ions per cm^2 at the probe position; the values are: 1.15 x 10^{14} ions cm^{-2} without the field and 7 x 10^{14} ions cm^{-2} with the field. It can also be noted that, with magnetic field, the arrival of the plasma at the probe and TOF at maximum of the ion signal occurs at earlier times than for the free ablation, which would seem to indicate a faster forward expansion, at least for some part of the flight from the target to the probe.

Figure 4 shows images of the plasma self-emission at various delays after the laser pulse. It should be noted that longer gate widths were used for the longer delays but the gain setting on the intensifier was kept constant. For free ablation the plume shows the normal, approximately semi-ellipsoidal, shape. From the images the aspect ratio, k_x, was estimated to be ~2.6. The plume front moves out from the target at ~3×10^6 cm s^{-1} which is in good agreement with the ion probe signal.

In the presence of the magnetic field the plume is distinctly different. Up to delays of ~300 ns the two cases are quite similar, but at 300 ns the plume in the magnetic field begins to look more cylindrical. The plume size at which the magnetic field is expected to begin to influence the plasma flow can be estimated by equating the ram pressure, due to the plasma flow, to the magnetic pressure. The magnetic pressure is $P_B = B^2/2\mu_0 = 4\times10^3$ N m^{-2}. For the free plume, the ram pressure in the Z direction at the probe position, at the time of maximum ion flux, is $P_R = n_i m_i v^2 = 1.5\times10^3$ N m^{-2}, where n_i is the ion density, m_i is the ion mass and v is the plasma velocity. For a 3-D inertial expansion, the ram pressure scales as (plume radius)$^{1/3}$ and its transverse component is $k^2_{x/y}$ times smaller than in the forward direction. Thus it is estimated that the ram pressure in the transverse direction (X or Y) will be equal to the magnetic pressure when the plume transverse radius is ~0.15 cm. This is close to the value of the transverse radius at 300 ns when influence of the magnetic field is first observed. From 300 ns onwards a rather flat conical flare is observed near the target surface.

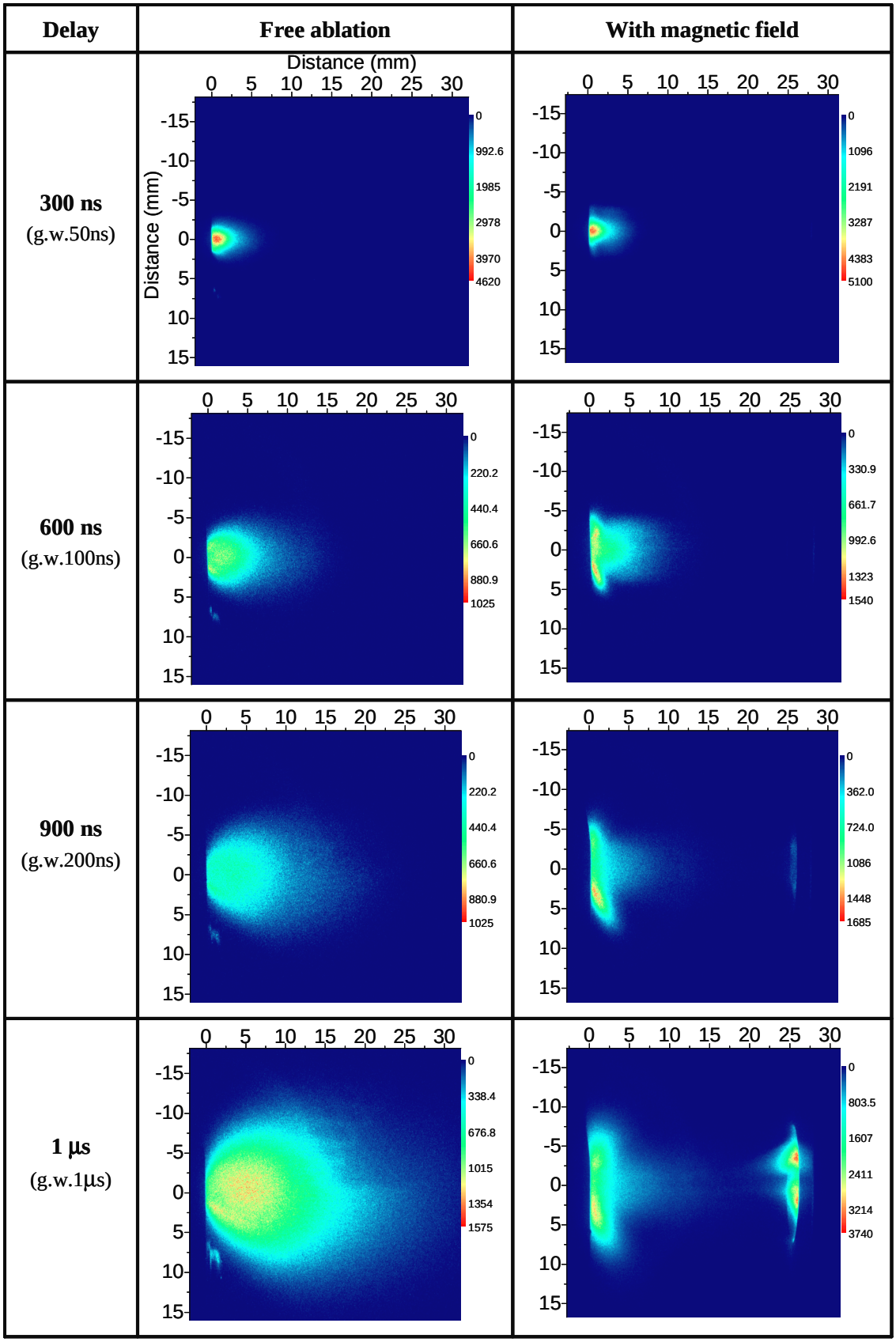

Figure 4: Time resolved images of the Cu plasma self-emission acquired with the ICCD without and with magnetic field. The time delays and the gate time-width, g.w., relative to each image are indicated in the first column. The images were acquired with the same gain.

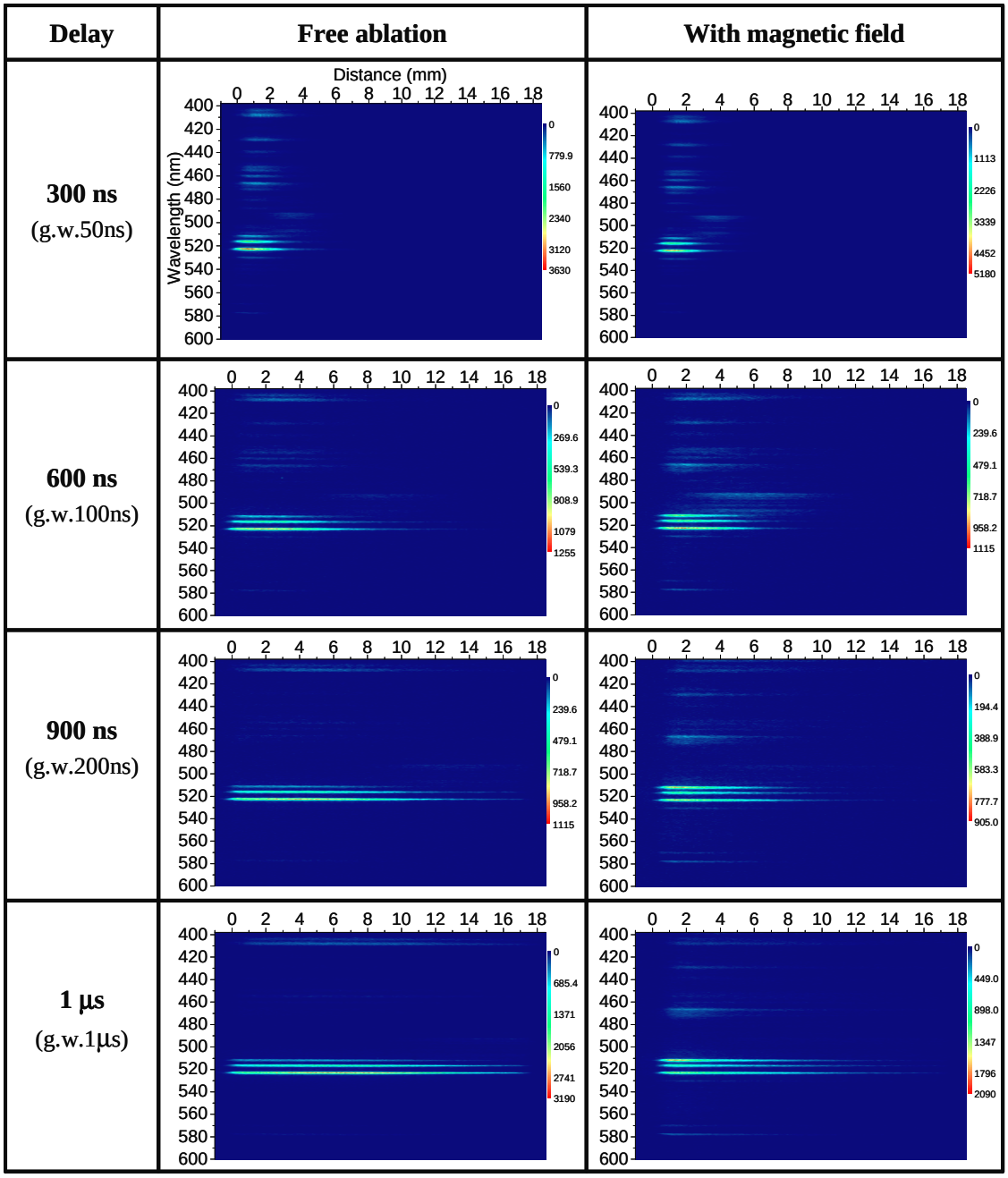

Figure 5: Time- and space-resolved spectra of the Cu ablation plume for various time delays, without and with magnetic field. The time delays and the gate time-width, g.w., relative to each image are indicated in the first column. The images were acquired with the same gain.

From 600 ns onward the cylindrical plume shape is more evident and the flare structure continues to develop. The emission from the region beyond 10 mm remains weak, but clearly plasma is moving through this region since its arrival at the hole in the magnet in front of the target can be observed. The light emission from the region at the surface of the magnet in front of the target first appears at ~600 ns, indicating a plasma velocity of ~5×10^6 cm s^{-1}, which is again consistent with the ion probe signal. At 1 µs delay the flare emission and the cylindrical plume between the magnets are very clear. In addition, intense emission is observed in the edge of the hole in the magnet in front of the target. In this region the magnetic field lines, which are axial in the region between the magnets, turn sharply to a more radial direction. There is then a component of plasma velocity normal to the field, and the

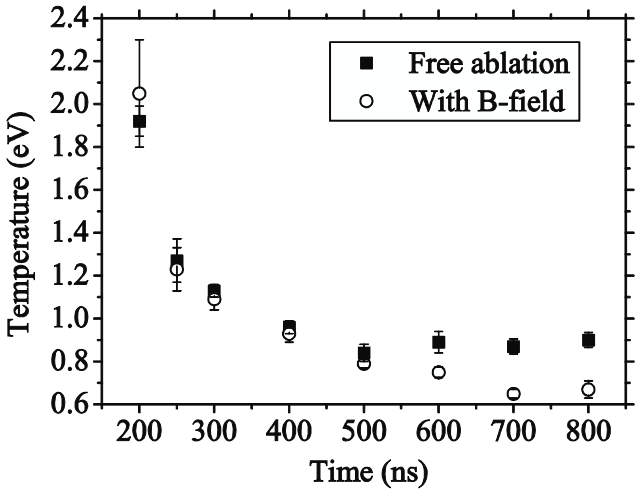

Figure 6: Temperature profile without and with magnetic field as a function of time at 2 mm from the target surface.

MHD activity will decelerate axial flow and heat the plasma. Strong radial confinement of the plume by the uniform field in the region between the magnets is expected and is similar to the confinement observed by Pisarczyk et al. [11], albeit for much hotter plasma and higher magnetic field. The X-ray images in that paper show an emission region of larger radius near the target, but not the flare described above. It seems that the flare emission may be due to an interaction near the target surface of the radial component of plasma velocity with magnetic field inducing an azimuthal current which heats the plasma in that region. However, full physical description requires detailed MHD modelling.

Figure 5 shows a comparison of space-resolved spectra without and with magnetic field which have been acquired simultaneously to the images in figure 4. From these spectral images it is possible to follow the expansion of the plume in the region from the surface (zero position) to 19 mm in front of the target. Thus the surface of the second magnet is not visible in these spectral images. The group of 3 strong lines have been identified as follows using the NIST tabulation [17], and are due to neutral Cu: Cu $3d^9 4s^2\ ^2D_{5/2}$ - $3d^{10}4p\ ^2P_{3/2}$ (510.69 nm), Cu $3d^{10}4p\ ^2P_{1/2}$ - $3d^{10}4d\ ^2D_{3/2}$ (515.32 nm) and Cu $3d^{10}4p\ ^2P_{3/2}$ - $3d^{10}4d\ ^2D_{3/2,\ 5/2}$ (522.15 nm, 521.81 nm). The weak feature near 491 nm is due to several Cu^+ $3d^9 4f$ - $3d^9 4d$ overlapping lines.

For free ablation the emission of the strong Cu lines moves away from the target with a velocity comparable to the values obtained from the ion probe and the time resolved imaging. At 1 μs the neutral emission is nearly uniform, though it should be remembered that in these space resolved spectra the emission is collected from a thin horizontal slice of the plume. In the spectral images at 400 and 600 ns it can be noted that the weak ion feature is moving away from the target more rapidly than the neutral lines. This is a normal feature of space resolved spectra from LPP [10], and is due to spatial variation of the state of the ionization over the plume.

In the presence of the magnetic field the spectra are different in several respects from the free ablation case. For most of the time interval examined, with the magnetic field present, the lines are particularly bright near the target, which may be due to the flare structure, and after about 10 mm the line intensity drops, in agreement with the images in figure 4. Furthermore, at times $\leq$600 ns, the intensity of the ionic lines at about 491 nm is distinctly stronger in the magnetic field. It seems that this is due to the concentration of plasma near the axis by the magnetic field. At times $\geq$600 ns, in the magnetic field case, there is an increase in the intensity of the 510 nm line relative to the 521/522 and 515 lines; as showed below, this is indicative of a lower electron temperature, T_e, since the 510 line is derived from a lower energy excited state.

It is possible to find T_e from the relative intensities of spectral lines derived for different excited states which are in local thermodynamic equilibrium (LTE). Using McWhirter's criterion [18] it was found that, for T_e ~1 eV, an electron number density, $N_e \geq 2\text{x}10^{15}$ cm^{-3} is required to maintain LTE between 4d ^{2}D and 4p ^{2}P multiplets. According to the plasma density profile derived from the ion

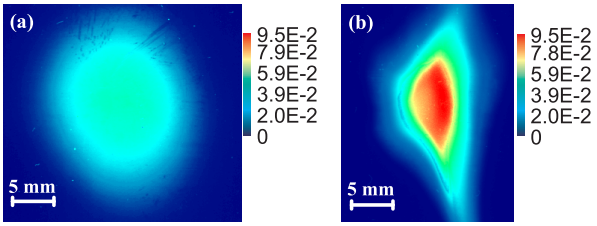

Figure 7: Images showing distribution of Cu deposition per laser pulse on glass slides at 2 cm from target: (a) without magnetic field, and (b) with magnetic field. The color scale indicates the thickness in nanometers.

signal in figure 3(a) in the free ablation case, it was found that at 2 mm from the target the McWhirter criterion is satisfied for delay time $\leq$800 ns. Since the plasma density is significantly higher when the magnetic field is present, LTE also apply in the same time and space domain as without the field. The evolution of the electron temperature was found by using a Boltzmann plot method [18, 19] to compare the relative intensity of the lines at 427, 458, 402-406, 510, 515 and 521-522 nm. Figure 6 shows the temporal variation of T_e at 2 mm from the target for both free ablation and ablation in the magnetic field. It can be seen that at late time ($\geq$600 ns) T_e is slightly lower in the presence of the magnetic field. The same behavior was found for a LPP expanding in a transverse magnetic field [10].

To investigate the influence of the magnetic field on the amount and distribution of ablated material flowing away from the target, thin film depositions were made on glass slides placed at 2 cm from the target. For free ablation 3000 laser shots were used, while in the magnetic field, where the deposition rate is higher, 750 shots were used. The deposition profile was found by measuring the optical transmission, around 515 nm, of the film with a calibrated flatbed scanner. The film thickness was found by comparing the measured transmission with a calculation using the XOP program [20] and assuming the bulk values for the complex refractive index of Cu. Figures 7(a) and (b) show the images of the depositions for free ablation and for the magnetic field case, respectively. It can be seen that in the magnetic field the deposition is restricted to a significantly smaller area, and the deposition rate in the centre of deposit is increased by a factor of ~2.6. It can be noted that while the magnetic field leads to a higher deposition rate over a smaller area, the spatially integrated deposition is about the same in both cases. In the magnetic field the shape of the deposition is less regular and shows fluted projections along the vertical direction, which may indicate the development of a plasma instability [21]. Finally it should also be noted that the magnetic field affects the expansion of both neutral and ionic components in the plasma. This behavior was already observed in [10] for a plasma expanding across a magnetic field.

Conclusion

It has been shown that when a low temperature LPP is directed along a moderate (0.3 T) magnetic field, the lateral expansion of the plasma is severely constrained. Both the ion yield and the deposition rate in the forward direction are strongly enhanced. These features are of interest for the development of laser plasma ion sources and PLD of thin films. A novel and intriguing conical flare develops near the ablation target. It will be of interest to use MHD modeling to find a deeper understanding of this interesting feature.

Acknowledgement

We acknowledge support from Science Foundation Ireland under research grant 07/RFP/PHYF143.

References

[1] Jordan R, Cole D and Lunney J G 1997 Pulsed laser deposition of particulate-free thin films using a curved magnetic filter, *Appl. Surf. Sci.* **109/110**, 403-407

[2] Tsui Y Y, Vick D and Fedosejevs R 1997 Guiding and confinement of a laser produced plasma by curved magnetic field *Appl. Phys. Lett.* **70**, 1953
[3] Radhakrishnan G and Adams P M 1999 Pulsed-laser deposition of particulate-free TiC coatings for tribological applications *Appl. Phys. A* **69** [Suppl.], S33-S38
[4] Weissmantel S, Rost D and Reisse G 2004 Magnetic field assisted increase of growth rate and reduction of particulate incorporation in pulsed laser deposited boron nitride films *Appl. Surf. Sci.* **197/198**, 494-495
[5] de Julian Ferandez C, Vassen J L and Givord D 1999 Thin film deposition by magnetic field-assisted pulsed laser assembly *Appl. Surf. Sci.* **138/139**, 150-154
[6] Kobayashi T, Akiyoshi H and Tachiki M 2002 Development of prominent PLD (Aurora method) suitable for high-quality and low-temperature film growth *Appl. Surf. Sci.* **197/198**, 294-303
[7] Rai V N, Rai A K, Yueh F and Singh J P 2003 Optical emission from laser-induced breakdown plasma of solid and liquid samples in the presence of a magnetic field *Appl. Opt.* **42**, 2085
[8] Harilal S S, Tillack M S, O'Shay B, Bindhu C V and Najmabadi F 2004 Confinement and dynamics of laser-produced plasma expanding across a transverse magnetic field *Phys. Rev. E* **69**, 026413
[9] Dirnberger L, Dyer P E, Farrar S R and Key P. H. 1994 Observation of magnetic-field-enhanced excitation and ionization in the plume of KrF-laser-ablated magnesium *Appl. Phys. A* 59, 311-316
[10] Pagano C, Hafeez S and Lunney J G 2009 Influence of transverse magnetic field on expansion and spectral emission of laser produced plasma *J. Phys. D: Appl. Phys.* **42**, 155205
[11] Pisarczyk T, Farynski A, Fiedorowicz H, Gogolewski P, Kuserz M, Makowski J, Miklaszewski R, Mroczkowski M, Parys P and Szczurek M 1992 Formation of an elongated plasma column by a magnetic confinement of a laser-produced plasma *Laser Particle Beams* **10**, 767-776
[12] Lisitsa V S and Skovoroda A A 2006 On a magnetic confinement of femtosecond laser pulse plasmas *Eur. Phys. J. D* **38**, 571-574
[13] http://www.comsol.com/
[14] Anisimov S I, Bauerle D and Luk'yanchuk B S 1993 Gas dynamics and film profiles in pulsed-laser deposition of materials *Phys. Rev. B* **48**
[15] Hansen T N, Schou J and Lunney J G 1999 Langmuir probe study of plasma expansion in pulsed laser ablation *Appl. Phys. A* **69** [Suppl.], S601-S604
[16] Doggett B and Lunney J G 2009 Langmuir probe charecterization of laser ablation plasmas *J. Appl. Phys.* **105**, 033306
[17] http://physics.nist.gov/PhysRefData/ASD/index.htm
[18] Shaikh N M, Rashid B, Hafeez S, Mahmood S, Saleem M and Baig M A 2006 Diagnostics of cadmium plasma produced by laser ablation *J. Appl. Phys.* **100**, 073102
[19] Amoruso S, Bruzzese R, Spinelli N and Velotta R 1999 Characterization of laser-ablation plasmas *J. Phys. B: At. Mol. Opt. Phys.* **32**, R131-R172
[20] http://www.esrf.eu/computing/scientific/xop2.1/extensions.html
[21] Anders A, Anders S and Brown I G 1995 Transport of vacuum arc plasmas through magnetic macroparticle filters *Plasma Sources Sci. Technol.* **4**, 1-12